Validation of MODIS-Aqua bio-optical algorithms for phytoplankton absorption coefficient measurement in optically complex waters of El Rincón (Argentina)

Ana L. Delgado[a,b,*], Valeria A. Guinder[a], Ana I. Dogliotti[c,d,e], Georgina Zapperi[a], Paula D. Pratolongo[a,f]

[a] *Instituto Argentino de Oceanografía (IADO), Consejo Nacional de Investigaciones Científicas y Técnicas - Universidad Nacional del Sur (CONICET-UNS), Bahía Blanca 8000, Argentina*
[b] *Departamento de Geografía y Turismo, Universidad Nacional del Sur (UNS), Bahía Blanca 8000, Argentina*
[c] *Universidad de Buenos Aires, Facultad de Ciencias Exactas y Naturales, Buenos Aires, Argentina*
[d] *CONICET -Universidad de Buenos Aires, Instituto de Astronomía y Física del Espacio (IAFE), Buenos Aires, Argentina*
[e] *Instituto Franco-Argentino para el Estudio del Clima y sus Impactos (UMI IFAECI/CNRS-CONICET-UBA), Buenos Aires, Argentina*
[f] *Departamento de Biología, Bioquímica y Farmacia, Universidad Nacional del Sur, Bahía Blanca 8000, Argentina*

A B S T R A C T

El Rincón is a highly productive area in the inner-shelf of the Argentine Sea, southern Buenos Aires Province (39°S–62.5°W; 41.5°S–60°W), regarded as the habitat for commercially valuable fish species and important for local artisanal fisheries. The aims of this work were to characterize for the first time the *in situ* absorption coefficient of phytoplankton ($a_{ph}(\lambda)$) in relation to phytoplankton composition and chlorophyll-*a* (Chl-*a*) concentration, and to evaluate the satellite retrieval of $a_{ph}(443)$ using two atmospheric correction algorithms and three bio-optical semi-analytical algorithms in order to define which is more suitable for the study area. A total of 28 oceanographic cruises were performed between November 2013 and March 2017 and the sampling included physical variables (temperature, salinity, suspended particulate matter, SPM), Chl-*a*, phytoplankton absorption and composition. The phytoplankton community was mainly dominated by chain-forming diatoms from the microplankton size class (40–80%), while a single coccolithophore, *Gephyrocapsa oceanica* (cell diameter < 10 μm) was a key component (up to 40%) of the nanoplankton. *In situ* Chl-*a* (mean 1.8 mg m^{-3}) and a_{ph} (443) (mean 0.052 m^{-1}) generally covariated with no clear seasonality. Their correlation was rather low (R^2 = 0.52) and with high scattering, in agreement with the high interannual variability of phytoplankton composition. Further, the relative low mean specific absorption coefficient of phytoplankton ($a_{ph}*$(443), 0.032 m^2 (mg Chl-*a*)$^{-1}$) and ($a_{ph}*$(676), 0.014 m^2 (mg Chl-*a*)$^{-1}$) denoted the presence of big cells and pigment packaging effect. Aside from the optical complexity of these waters, reasonable results were found using the Quasi Analytical Algorithm in retrieving a_{ph} coefficient (R^2 = 0.55, Bias = 19%) and switching the atmospheric correction algorithm depending on the distance to the coast, the depth and turbidity. The results found in this paper present for the first time the phytoplankton composition and absorption of algal material characteristics and the derived implication on the performance of bio-optical algorithms in the optically complex waters of El Rincon.

1. Introduction

Marine phytoplankton play a central role in the carbon cycle by yielding ca. 50% (~50 Gt C/year) of the global primary production (Longhurst et al., 1995; Field et al., 1998). By their position at the base of marine food webs, these communities shape biogeochemical cycles, carbon export from the euphotic zone to the deep ocean and energy fluxes through ecosystems (Margalef, 1978; Finkel et al., 2009; Van de Waal et al., 2010). In fact, phytoplankton growth is essential to support fisheries and for the benthic-pelagic coupling in coastal shelf areas

* Corresponding author at: Instituto Argentino de Oceanografía (IADO), Consejo Nacional de Investigaciones Científicas y Técnicas - Universidad Nacional del Sur (CONICET-UNS), Bahía Blanca 8000, Argentina.
E-mail addresses: aldelgado@iado-conicet.gob.ar (A.L. Delgado), vguinder@criba.edu.ar (V.A. Guinder), adogliotti@iafe.uba.ar (A.I. Dogliotti), gzapperi@criba.edu.ar (G. Zapperi), paulapra@criba.edu.ar (P.D. Pratolongo).
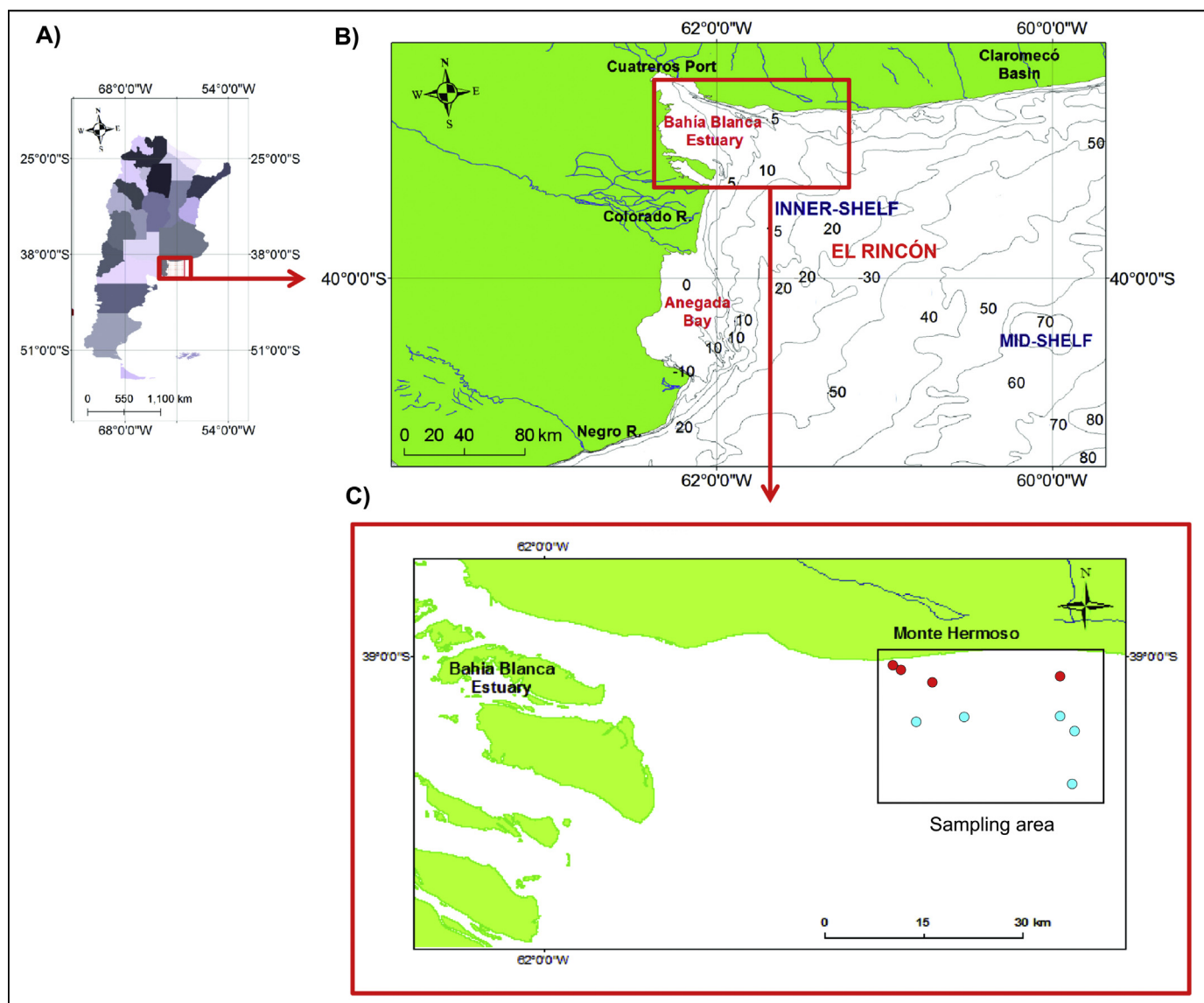
Fig. 1. Location of study area. A) Argentina, B) Inner and mid shelf of southern Buenos Aires Province, C) *In situ* sampling area. Red spots stand for very coastal stations (distance < 10 km, z ≈ 5 m) and light cyan spots for further stations (distance > 10 km, z > 10 m). (For interpretation of the references to color in this figure legend, the reader is referred to the web version of this article.)

(Legendre, 1990). Fluctuations in phytoplankton biomass, such as blooms events, respond to changes in the availability of light and nutrients. Further, in temperate environments, these events are triggered by the increase in radiation, temperature and water column stability during spring, while nutrient depletion and zooplankton grazing pressure determine their collapse (Sommer, 2012). The optical characteristics of water masses reflect these changes in phytoplankton biomass, phytoplankton types and community structure (*e.g.* Bouman et al., 2003; Bricaud et al., 2004; Sathyendranath et al., 2004). Therefore, optical remote sensing provides an economic tool to synoptically study the phytoplankton spatial distribution and temporal variability in marine systems.

The absorption coefficient of phytoplankton ($a_{ph}(\lambda)$) conveys information on the biomass and physiological state of phytoplankton. Variability of $a_{ph}(\lambda)$ may result from changes in phytoplankton cell concentration, the pigment composition of different species, or the combination of both (*e.g.* Morel and Bricaud, 1981; Stramski et al., 2001; Ferreira et al., 2013a). Pigment packaging is a widely known source of $a_{ph}(\lambda)$ variability, which depends on cell size and intracellular concentration of pigments (Morel and Bricaud, 1981;

Sathyendranath et al., 2001; Ciotti et al., 1999; Ferreira et al., 2013a). The absorption by phytoplankton is one the most important inherent optical properties of seawater affecting the spectral reflectance of the ocean. Thus, this property is relevant to ecological studies and applications associated with remote sensing (*e.g.* Morel and Bricaud, 1981; Sathyendranath et al., 2001), especially in turbid coastal waters which have been less studied.

The reflectance spectra of water masses greatly depend on the inherent optical properties (IOPs), which result from the different concentrations of optically active components in seawater (Gordon et al., 1988). Thus, the development of reliable algorithms for the retrieval of biophysical information from optical images depends on the understanding of the spectral absorption and scattering of dissolved and suspended substances in seawater (*e.g.* Stramski et al., 2004; Clemenston et al., 2004; Ahn et al., 2006). Even though Chl-*a* concentration is extensively used as a proxy of phytoplankton biomass, its retrieval is often problematic in optically complex coastal waters. The use of optical indexes such as $a_{ph}(\lambda)$, instead of Chl-*a,* for phytoplankton biomass estimation is increasingly explored (*e.g.* Marra et al., 2007; Lee et al., 2011; Hirawake et al., 2011; Shang et al., 2011, 2014). Optical

indexes offer an advantage because the ocean color depends on the spectral absorption and scattering properties of seawater and its optically active dissolved and particulate components, not just pigment concentrations (Gordon et al., 1988).

Several efforts have been made worldwide to develop general models for deriving information of phytoplankton cell size and pigment composition from their absorption spectra and from the specific phytoplankton absorption coefficient that relates $a_{ph}(\lambda)$ and Chl-*a* concentration (Bricaud et al., 1995, 2004; Ciotti et al., 2002; Brewin et al., 2012). In the Argentine Sea, South Western Atlantic, bio-optical properties of sea water have been studied in mid-shelf areas (Lutz et al., 2006), in the San Matías Gulf (Williams et al., 2013), and in the outer-shelf (Ferreira et al., 2013a, 2013b; Segura et al., 2013). However, the information remains scarce regarding field estimates of bio-optical parameters in more coastal and optically complex waters in this region of the Atlantic.

The inner-shelf of southern Buenos Aires Province at ~39.18˚S 61.28˚W (usually called El Rincón) is characterized for presenting turbid waters all year round, high variability of salinity and water temperature and for being influenced by the estuarine plume coming from the Bahía Blanca Estuary (Delgado et al., 2017). The constant winds prevailing from the north and northwest allow the continual mixing of the water column (Piccolo, 1998). This coastal area, which is the habitat of commercially valuable fish species and important for local artisanal fisheries (Carroza et al., 2009; López Cazorla et al., 2014), has not been yet studied enough as to understand the basic ecosystem functioning. Here we analyzed a multivariable dataset of physical, optical and biological properties of surface waters in El Rincón area, to assess their dynamics and build the basis for future suitable bio-optical algorithms. The permanent monitoring area is adjacent to Monte Hermoso city (Fig. 1), where data acquisition has started in November 2013 with the support of local artisanal fishermen. The specific aims of the present work were (i) to characterize and investigate the *in situ* $a_{ph}(\lambda)$ in relation to the phytoplankton composition and Chl-*a* concentration and (ii) to evaluate the satellite retrieval of $a_{ph}(\lambda)$ using two atmospheric correction algorithms and three bio-optical semi-analytical algorithms in order to define which is more suitable for the study area.

2. Materials and methods

2.1. In situ data

2.1.1. Sampling

A total of 28 oceanographic cruises were performed between November 2013 and March 2017 (Table 1) in the permanent sampling area located in El Rincón (39˚S–62.5˚W; 41.5˚S–60˚W, Fig. 1). Sampling was usually performed around noon, on board of local artisanal fishing boats. Artisanal fishers in the area have several fixed sampling sites, but they visit one single site per day. Thus, for a given sampling date, sampling was performed once, at one of the fishing sites (Fig. 1C). Surface water samples were obtained with a Van Dorn bottle from which Chl-*a* concentration (mg m^{-3}), phytoplankton absorption coefficient ($a_{ph}(\lambda)$; m^{-1}), suspended particulate matter (SPM) (mg l^{-1})and phytoplankton abundance (cells l^{-1}) were determined. Physico-chemical properties of surface waters (temperature, salinity and pH) were measured *in situ* with an YSI pro1030 (Table 1). For quantitative analysis of phytoplankton and cell size estimations, surface water samples (250 ml bottles) were fixed with acidified Lugol´s solution at 1% final concentration. For the taxonomic identification of phytoplankton, samples were collected using a Nansen 30 μm net and preserved with formaldehyde (final concentration 4%).

2.2. Analytical methods

Chlorophyll-*a* (Chlorophyll-*a* + phaeopigments, hereafter Chl-*a*)

concentrations were estimated by filtering between 100 and 200 ml of seawater though 0.7 μm Whatman GF/F filters, depending on the water turbidity. Immediately after filtration, the filters were wrapped in aluminum foil and stored in an ultrafreezer at −80 °C until analysis. Pigment extractions were performed in acetone 90% (5 ml) during 24 h at −20 °C in the dark. Chl-*a* concentrations were finally determined following the fluorometric method of Holm-Hansen et al. (1965), using a spectrofluorophotometer Shimadzu RF 5301 PC, properly calibrated with pure Chlorophyll-*a* from the cyanobacteria *Anacystis nidulans* (Sigma C-6144).

For $a_{ph}(\lambda)$ estimations, water samples were filtered and stored using the same procedure described for Chl-*a* samples. The particulate absorption spectra were estimated through the quantitative technique developed by Mitchell (1990), using a spectrophotometer Jasco UV–Vis 630 in the 300–800 nm spectral range. After the total particulate matter absorption was measured, the sample filters were subjected to methanol extraction and then re-scanned to obtain estimates of the non-algal particulate absorption (Kishino et al., 1985; Mitchell et al., 2000). The spectral absorption coefficient of the total particulate matter (a(λ)) and non-algal material ($a_{nap}(\lambda)$) were derived from the quadratic equation of Mitchell (1990) performing the correction of the null value absorption (790–800 nm) and the path length amplification factor. The phytoplankton absorption coefficient ($a_{ph}(\lambda)$) was calculated subtracting $a_{nap}(\lambda)$ from a(λ). $a_{ph}(\lambda)$ data for the period between 30th November 2013 and 14th November (1st year of sampling) are not available due to technical problems with the spectrophotometer.

Suspended particulate matter (SPM) was obtained by filtering 500 ml through 0.7 μm Whatman GF/F filters, which were combusted and pre-weighed. After filtration, filters were oven dried at 60 °C for 24 hs and re-weighed (Van der Linde, 1998). Turbidity was measured with a HACH 2100Q IS portable turbidimeter.

For quantitative analysis of phytoplankton, individual cells were identified and counted under a Wild M20 inverted microscope according to the procedures described by Hasle (1978). Subsamples of 10 ml (sometimes 5 ml due to the large amounts of suspended sediments) of seawater preserved with Lugol were settled in Utermöhl sedimentation chambers for 24 h. The entire chamber was then analyzed under magnification of 40×, and phytoplankton cells > 5 μm were counted. Since flagellates generally lose their flagella by the addition of fixatives, unidentified flagellates and round-shaped organisms with or without flagella were included in a single group called "flagellates" during cell counting and classified according to their size. Concerning dinoflagellates, the species of the genera *Protoperidinium, Gyrodinium* and some *aff. Gymnodinium* were excluded for the estimation of phytoplankton abundance and biomass, as they are mostly heterotrophs (Hoppenrath and Debres, 2009; Guinder et al., 2018). Phytoplankton species identification was done from the net samples under a Zeiss Standard R microscope and a Nikon Eclipse microscope, using phase contrast, differential interference contrast (DIC) and magnification of 100×.

Cell dimensions were measured using an ocular micrometer. Afterwards, phytoplankton cell volumes (in μm^3) were calculated assigning simple geometric shapes to species according to Hillebrand et al. (1999) and transformed into carbon content (pg C cell^{-1}) using two different carbon-to-volume ratios, one for diatoms and one for all the other algae groups (Menden-Deuer and Lessard, 2000). Finally, total phytoplankton biomass (μg C l^{-1}) was estimated for each sampling date according to the phytoplankton abundance.

2.3. Satellite data

The $a_{ph}(\lambda)$ was obtained from the Moderate Resolution Imaging Spectroradiometer (MODIS) on board Aqua satellite. Daily level 1A data at 1.1 km spatial resolution were downloaded from the Ocean Color web site (http://oceancolor.gsfc.nasa.gov). The extracted L1A files for the study area were processed using SeaDAS 7.4 software to

Table 1

Details of the cruises performed in the study area between November 2013 and February 2017. Gray shadow stands for measured variables. MH = Monte Hermoso. CS = conductivity and salinity; pH; SPM = suspended particulate matter concentration; Chl-a = chlorophyll-a concentration; a_{ph} = phytoplankton absorption coefficient; T = turbidity; PC = Phytoplankton composition.

Cruisename	Date	MODIS-Aqua	CS	pH	SPM	Chl-a	a_{ph}	PC	T
MH1	30 November 2013								
MH2	27 January 2014								
MH3	6 February 2014								
MH4	27 March 2014								
MH5	31-may-14								
MH7	13 November 2014								
MH8	16 November 2014								
MH9	7 December 2014								
MH10	21 January 2015								
MH11	28 January 2015								
MH12	21 February 2015								
MH13	27 March 2015								
MH14	25 April 2015								
MH15	16 July 2015								
MH16	3 September 2015								
MH17	1 November 2015								
MH18	25 February 2016								
MH21	16 June 2016								
MH22	17 June 2016								
MH23	23 June 2016								
MH25	2 September 2016								
MH26	27 September 2016								
MH27	18 November 2016								
MH28	18 January 2017								
MH29	19 January 2017								
MH30	28 January 2017								
MH31	12 February 2017								

obtain L2 products. In order to evaluate the estimates, two atmospheric correction algorithms were applied: (1) the NASA standard algorithm (STD) based on the assumption of black pixel in the near infrared (NIR) bands with modifications to account for the water-leaving reflectance contribution for more coastal moderately turbid waters (Stumpf et al., 2003; Bailey et al., 2010) and (2) the alternative algorithm developed for turbid waters that uses black pixel assumption in the short-wave infrared (SWIR) (Wang and Shi, 2007; Wang et al., 2009). Given the presence of turbid waters in the region the high total radiance mask (HILT) was not applied and the cloud-masking was performed using the Rayleigh-corrected reflectance (dimensionless) at 2130 nm and a threshold of 0.018. Three a_{ph}(443) products were derived using the generalized IOP algorithm (GIOP, Franz and Werdell, 2010; Werdell et al., 2013), the Graver-Siegel-Maritorena algorithm (GSM, Maritorena et al., 2002) and the Quasi analytical algorithm (QAA) (Lee et al., 2002).

2.4. Match-up protocol

The match-up procedure consisted in extracting a box of 3 × 3 pixels, centered in the location of the *in situ* measurements, and to calculate the mean, standard deviation and coefficient of variation of the product in order to test the spatial homogeneity of the variable in the box at the validation point (Bailey and Werdell, 2006). A match-up was accepted only if more than 6 pixels of the box were valid considering the flags proposed by Bailey and Werdell (2006) (Jamet et al., 2011). Then, a spatial uniformity criterion was applied based on the coefficient of variation (cv), defined as the ratio of the standard deviation to the mean pixel value of the box, if cv > 0.3 the data is discarded (Bailey and Werdell, 2006). The time difference between the satellite overpass and the *in situ* measurement were within ± 3 hs of the satellite overpass. In addition, a manual quality control procedure was performed, which consisted in visually checking on satellite images that match-ups were not located in cloud or land borders, in order to avoid erroneous satellite estimations of $a_{ph}(\lambda)$.

2.5. Statistical analysis

In order to evaluate the performance of the MODIS-Aqua a_{ph}(443) products, a statistical analysis was performed comparing the *in situ* to the satellite data. At first, *in situ* and satellite-derived data were logarithmically transformed given that bio-optical data tend to be log-normally distributed (Campbell, 1995). Linear regressions were carried out and the slope, intercept, and coefficient of determination (R^2) were calculated. The statistical parameters used for the evaluation were the root-mean-square error (RMSE) (Eq. (1)), BIAS (Eq. (2)) and the relative
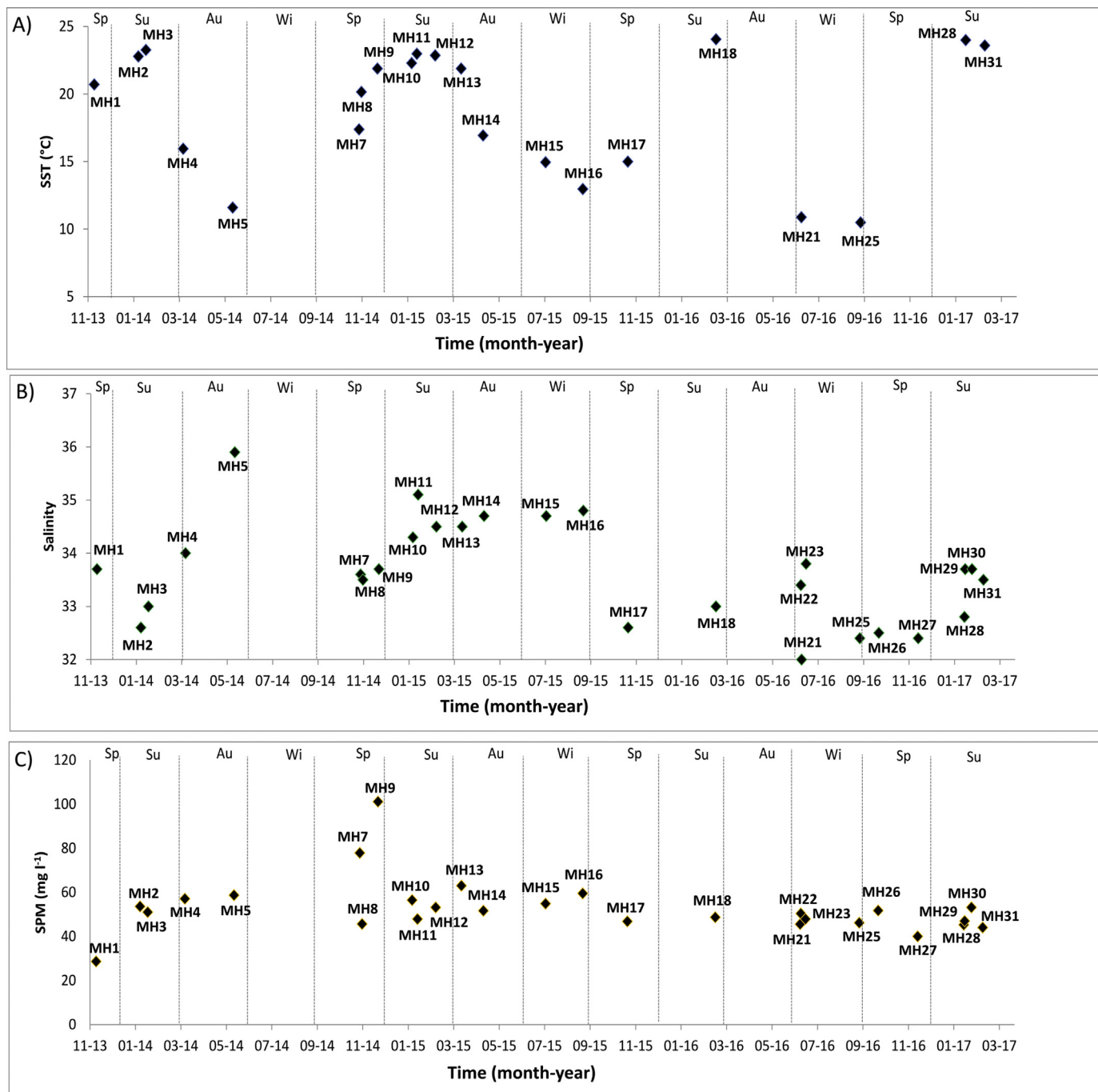
Fig. 2. Environmental conditions of the study area: A) Sea surface temperature (°C); B) Sea surface salinity; C) Surface suspended particulate matter (SPM) (mg l⁻¹). Vertical dashed lines delimit seasons: Spring (Sp); Summer (Su); Autumn (Au); Winter (Wi).

error (RE) (Eq. (3)), defined as:

$$RMSE = \sqrt{\frac{1}{n} \sum [b - a]^2}$$ (1)

$$BIAS = \frac{1}{n} \sum (b - a) x 100$$ (2)

$$RE = \frac{b - a}{a}$$ (3)

where a is the measured parameter, b the satellite estimates and n the number of match-ups.

3. Results and discussion

3.1. Environmental setting

Considering the three-year sampling period, the sea surface temperature displayed marked seasonality and high thermal amplitude (14 °C) (Fig. 2A). It is important to highlight that no data were obtained during austral winter (July to August), when the lowest water temperatures occur. The maximum temperature was registered in summer 2016 (24 °C) and the minimum in June 2016 (10 °C). Previous studies have ascribed the high seasonal thermal amplitude of the study area (16.6 °C) to the compound effects of the shallow water column and the plume of the Bahía Blanca Estuary (Delgado et al., 2014, 2017).

Overall, El Rincón area presents high mean salinity (35) with strong seasonal and inter annual variability related to the influence of: the Negro and Colorado rivers, the Bahía Blanca Estuary (BBE), the southward advection of San Matías Gulf waters, and the local rainfall (Lucas et al., 2005; Delgado et al., 2017). In this study, salinity oscillated between 32 (June 2016) and 36 (May 2014) (Fig. 2B), with a mean value of 33.6. Even though a clear seasonality was not detected, generally high values were observed in autumn and minimum in spring in agreement with previous studies (Lucas et al., 2005; Delgado et al., 2017).

Suspended particulate matter (SPM, mg l^{-1}) was usually high for the studied period, with a mean value of 54.4 mg l^{-1}, ranging between 28.6 (MH1; November 2013) and 101 mg l^{-1} (MH9; December 2014). A clear seasonal pattern was not detected, although the minimal mean value was observed in winter (50 mg l^{-1}) and the maximal in spring (60 mg l^{-1}) (Fig. 2C). Based on the sediment mineralogy (Perillo and Cuadrado, 1990), the Bahía Blanca Estuary seems to be the major source of suspended sediments to the study area, which has been regarded as turbid (24–64 NTU, Delgado et al., 2017).

3.2. Phytoplankton composition

Here we analyzed only the phytoplankton community > 5 μm. This community was highly dominated by diatoms over the studied period, reaching between ca. 40–90% of the total abundance in each sampling date (Fig. 3A). Diatoms were the most abundant and diverse group, represented by a wide range of cell sizes and shapes (*e.g. Chaetocerossocialis* with a biovolume of 70 μm^3 and a carbon content of 9 pg C l^{-1}; whereas *Odontellasinensis* with 230,000 μm^3 and 6423 pg C l^{-1}). However, the relative dominance of large diatoms in the samples explains the high biomass (> 78%) reached over the studied period compared to other phytoplankton groups, such as dinoflagellates and small flagellates (Fig. 3B). The most abundant and frequent diatom species in the plankton were: *Asterionellopsis glacialis, Cymatosirabelgica, Thalassionemanitszchioides, Odontellaaurita, O. sinensis, Attheyaarmatus, Guinardiadelicatula, Paraliasulcata, Skeletonemacostatum, Pseudo-nitschia spp., Actinocyclus sp., Chaetocerossocialis, C. lorenzianus, C. dydimus, Cerataulinapelagica, Thalassiosira spp., Cyclotella sp., Rizosolenia spp., Coscinodiscus* spp. and other pennate diatoms of the genera *Nitszchia, Navicula* and *Fragilariopsis*.

Microplanktonic diatoms commonly dominate in highly turbid, nutrient-rich and turbulent temperate coastal waters (Litchman et al., 2012) (Fig. 3C). The particular ecological features of this phytoplankton group (silicified cell wall and metabolic adaptations to high nutrient-low underwater light conditions) confers them higher tolerance against turbulent stress and zooplankton grazing and fast population growth (blooms) in response to pulses of light and nutrients over other phytoplankton groups, *e.g.* dinoflagellates (Litchman et al., 2012). The high frequency of benthic and ticopelagic diatom species found in surface waters in this study (*Rhaphoneisamphiceros, Cylindrothecaclosterioum, Paraliasulcata, Cymathosirabelgica, Gyrosigma* sp. and *Nitzschia* spp.), together with the high levels of suspended sediments and aggregates in the samples, correspond to turbid and mixed conditions. This is concomitant with the effects of strong winds and waves typical in the studied area (Delgado et al., 2012), where the water column may experience intense vertical resuspension of bottom sediments plus the influence of turbid waters coming from the Bahia Blanca Estuary (Delgado et al., 2017).

The second most abundant phytoplankton group, coccolithophores (Fig. 3A), was represented by a single species, *Gephyrocapsaoceanica*, which corresponds to the nanophytoplankton size class. Only on one date (25 April 2015), diatoms were not the dominant group, and the coccolitophorid *G. oceanica* reached 53% of the phytoplankton abundance (0.34 × 10^5 cells L^{-1}). In spite of the large numerical predominance of this coccolithophore, its contribution to total biomass was moderate (18%) because of its small size (diameter 6–12 μm and 31

– 201 pg C l^{-1} of biomass). *Gephyrocapsaoceanica* has been encountered as a coastal species in the large area of El Rincón (Negri et al., 2013; Segura et al., 2013; Guinder et al., 2018). Further, it has been found that this species produces important blooms in coastal areas being an important source of carbon (Rohdes et al., 1995; Kai et al., 1999).

Other groups represented in the phytoplankton assemblages were small phytoflagellates (5–20 μm), dinoflagellates, and the xantophyceae represented only by one large single species, *Ophiocytium* sp. The group of flagellates includes cryptophytes, prasinophytes, prymnesiophytes and green algae such as euglenophytes and other unidentified phytoflagellates. The most commonly identified species were the euglenophyte *Eutreptiella* sp. and the silicoflagellate*Dictyocha speculum*. The dinoflagellates were represented by a few species, where *Heterocapsa sp., Scrippsiellatrochoidea* sp. and *Prorocentrumaff.minimum* were the most representative ones over the sampled period. It is worth noting that in this study, the phytoplankton cells < 5 μm were not counted (pico- 0.2–2 μm and ultraphytoplankton 2–5 μm), which has been regarded as highly important components of phytoplankton in the area. In fact, previous studies indicated that small phytoplankton *e.g. Synechococcus* and *picophytoeukariots* reach high abundances in February in El Rincón area (Negri et al., 2013).

3.3. Phytoplankton temporal variability

The phytoplankton abundance and species succession did not display seasonality over the three studied years. The total abundance of cells > 5 μm ranged between 0.5 × 10^5 and 2.8 × 10^5 cells l^{-1}, and large diatoms corresponding to the size fraction of microplankton were highly represented all year round. Nevertheless, we are aware that the sampling frequency performed in this study might not be enough to track gradual and continuous changes in the phytoplankton populations. The absence of apparent phytoplankton seasonality suggests that local environmental forces such as strong permanent winds, water mixing and turbidity, and eventually low light penetration, might modulate the phytoplankton development, instead of the deepening of the euphotic zone due to spring stratification (Sommer, 2012). Moreover, as dissolved inorganic nutrients revealed no limitation (Redfield et al., 1963; Brzezinski et al., 1998) for phytoplankton growth, turbidity likely results the most important factor regulating phytoplankton variability in this coastal system, where suspended sediments play a key role in the attenuation of light penetration all-year-round, as in the adjacent Bahía Blanca Estuary (Guinder et al., 2009). In this context, the rather low biomass to chlorophyll ratio of phytoplankton (mean value ± standard deviation: 200.2 ± 172.3) may be a consequence of low underwater light availability, in accordance to cell's photo-acclimation mechanisms under low light and nutrient replete conditions (Wang et al., 2009).

3.4. Phytoplankton absorption in complex coastal waters: influence of cell size

During the studied period, Chl-*a* mean value was 1.8 mg m^{-3} and ranged between 0.5 and 2.85 mg m^{-3} (Fig. 4A), while the mean value of a_{ph} (443) was 0.052 m^{-1}, fluctuating between 0.02 (February 2017) and 0.13 m^{-1} (December 2014) (Fig. 4B). A moderate significant correlation between both parameters was observed (r = 0.65, p < 0,01).

The variations of a_{ph}(443) and a_{ph} (676) as function of Chl-*a* (chlorophyll-*a* plus phaeopigments) concentration are shown in Fig. 5A. It can be observed that a_{ph}(443) increases with Chl-*a* according to a power function as has been observed in previous studies (*i.e.* Bricaud et al., 1995, 2004; Wang et al., 2005; Ferreira et al., 2013b). The least square fit of our data set provides the following function:

$$a_{ph}(443) = 0.0106(Chla)^{1.6095}$$

(4)

with a R^2 of 0.59 considering 21 samples. The data set presented here is
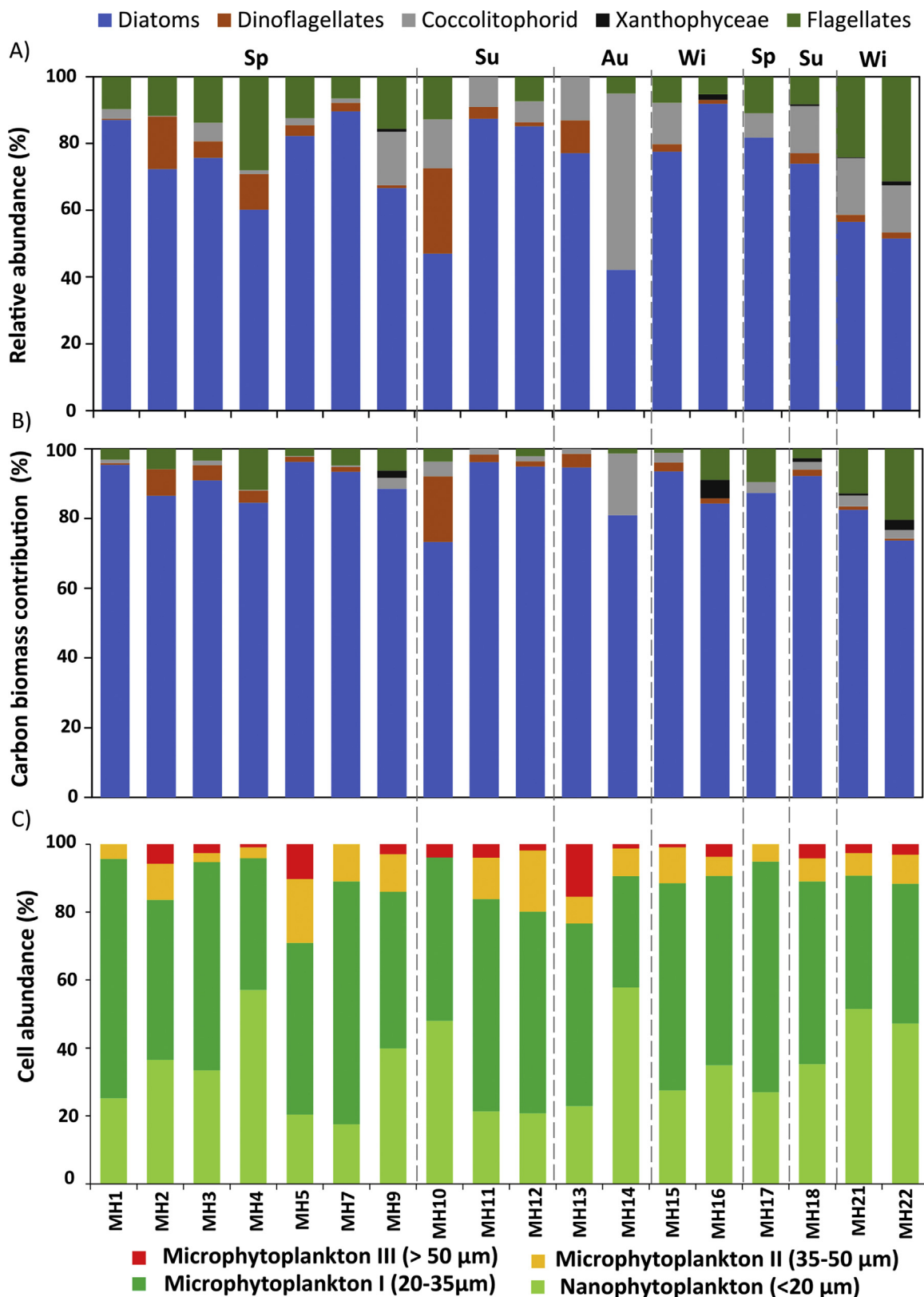
Fig. 3. A) Relative cell abundance of main phytoplankton functional groups; B) Carbon biomass contribution of main functional groups and; C) Relative cell abundance of main size fractions during the sampling period in the study area. Percentages were taken considering 100% as the total phytoplankton community > 5 μm. Vertical dashed lines delimit seasons: Spring (Sp); Summer (Su); Autumn (Au); Winter (Wi).

considerably biased toward lower values compared with the previously mentioned studies. When comparing our results with relationships found in the literature, in this study the closer relationship (at 443 nm) was found with Wang et al. (2005) (Wa05), although the values are lower and the slope is considerably different. The relationships based on two size fractions, nanophytoplankton (FNa) and
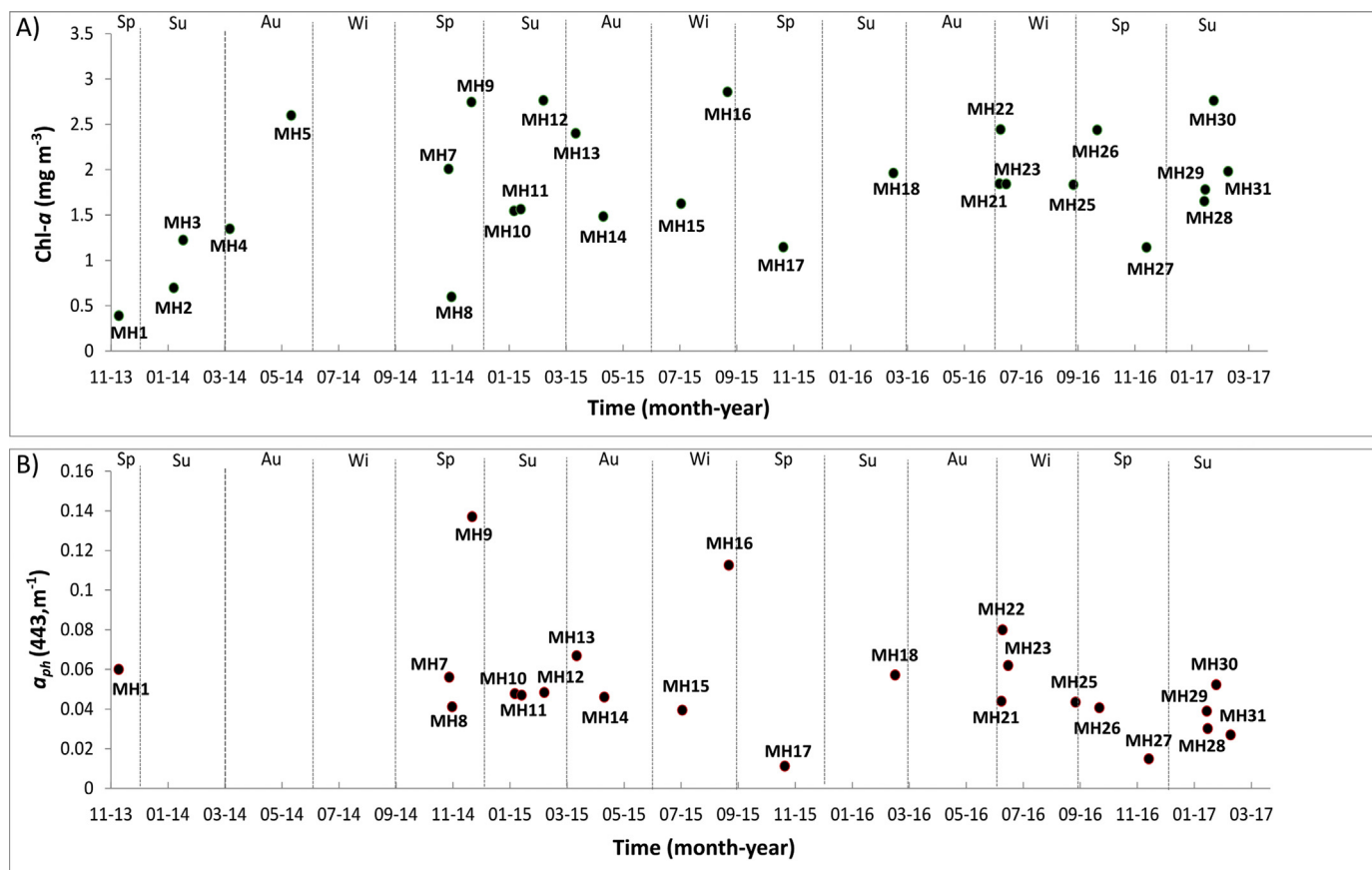
Fig. 4. Daily *insitu* values of A) Chl-*a* (mg m^{-3}) and B) a_{ph}(443) (m^{-1}). Vertical dashed lines delimit seasons: Spring (Sp); Summer (Su); Autumn (Au); Winter (Wi).

microphytoplankton (FeMI), described in Ferreira et al. (2013b), and the relationship described in Bricaud et al. (1995) and Bricaud et al. (2004), depart even further from our results (Fig. 5). The main source of differences might be attributed to the cell size structure of the phytoplankton assemblages. Except for the FeMI and Wa05, the other relationships were found in waters where the main phytoplankton group size was the nanophytoplankton, whereas in our study area the abundance of microphytoplankton dominated the samples as previously reported by Guinder et al. (2018), even though the ultraphytoplankton has been previously addressed to be in February 2011 the predominant functional group of the study area (Negri et al., 2013), but unfortunately was not measured in the present study. Also, the species observed in the study area probably differed from the ones in the mentioned studies, which may lead to different pigment composition resulting in an additional source of difference.

At longer wavelengths (676 nm) the scatter of the data increases and the R^2 diminished:

$$a_{ph}(676) = 0.0099(Chla)^{0.8826} \tag{5}$$

The exponent of the function of this study is similar to the ones reported in Ferreira et al. (2013a) for the two size fractions (0.74 for FNa and 0.62 for FeMI), but the values are closer to Bricaud et al. (1995) relationship (0.159). Since at this wavelength (676 nm) the contribution to absorption of pigments other than Chl-*a* is considered to be negligible, the main source of differences could be the larger phytoplankton cell sizes found in our study compared to other regions, including the Patagonian case 1 waters studied by Ferreira et al. (2013b). This is expected, since the main size fraction of our study area is microplankton (cells > 20 μ, mainly characterized for chain-forming diatoms) which are common in coastal turbulent waters as discussed before.

The specific absorption coefficient of phytoplankton, $a_{ph}^*(\lambda)$,

defined as the ratio of a_{ph} to Chl-*a* exhibited high variability, varying from 0.009 to 0.15 m^2 (mg Chl-*a*)$^{-1}$ at 443 nm, and from 0.007 to 0.05 m^2 (mg Chl-*a*)$^{-1}$ at 676 nm (Fig. 6A-B), as observed in other optically complex waters (Dupouy et al., 2010). Variations in a_{ph}^* have been previously associated with phytoplankton pigment composition and the packaging effect. Larger cell sizes, like those found in diatom-dominated phytoplankton communities, may lead to intracellular shading by pigment packaging effect resulting in a decreased efficiency in pigment cells absorption compared to the potential absorption of the same amount of pigments in solution (Morel and Bricaud, 1981). Thus, relatively high Chl-*a* and low $a_{ph}^*(\lambda)$ are associated with larger cells which are more affected by pigment packaging (Bricaud et al., 1995; Ferreira et al., 2013b), and relatively low Chl-*a* and high $a_{ph}^*(\lambda)$ are indicative of phytoplankton communities containing small cells. The generally accepted values of $a_{ph}^*(\lambda)$ in the red band of non-packaged pigments, where the influence of accessory pigments is minimal, range between 0.023 and 0.029 m^2 (mg Chl-*a*)$^{-1}$ (Johnsen et al., 1994; Moisan and Mitchell, 1999). Meanwhile in our study, the mean $a_{ph}^*(676)$ was 0.014 m^2 (mg Chl-*a*)$^{-1}$, evidencing pigment packaging in agreement with findings in other coastal waters (Wang et al., 2005; Vantrepotte et al., 2007).

The variations of a_{ph}^* as a function of Chl-*a* are shown in Fig. 7A and 7Bat two wavelengths, in the blue (443 nm) and the red (676 nm)portions of the spectrum. It can be observed that various $a_{ph}^*(\lambda)$ were found for a given Chl-*a* value and a determined $a_{ph}^*(\lambda)$ is associated to various Chl-*a* concentrations, but no significant correlation or clear relationship was found between $a_{ph}^*(\lambda)$ and Chl-*a* as in other study areas (Ferreira et al., 2013b). The scatter and variations of a_{ph}^* values for a given Chl-*a* concentration could be a result of a combination of different cell sizes with differential packaging effect, as well as differences in pigment composition (Hoepffner and Sathyendranath, 1992) as phytoplankton communities changed through time (Fig. 3A). It is
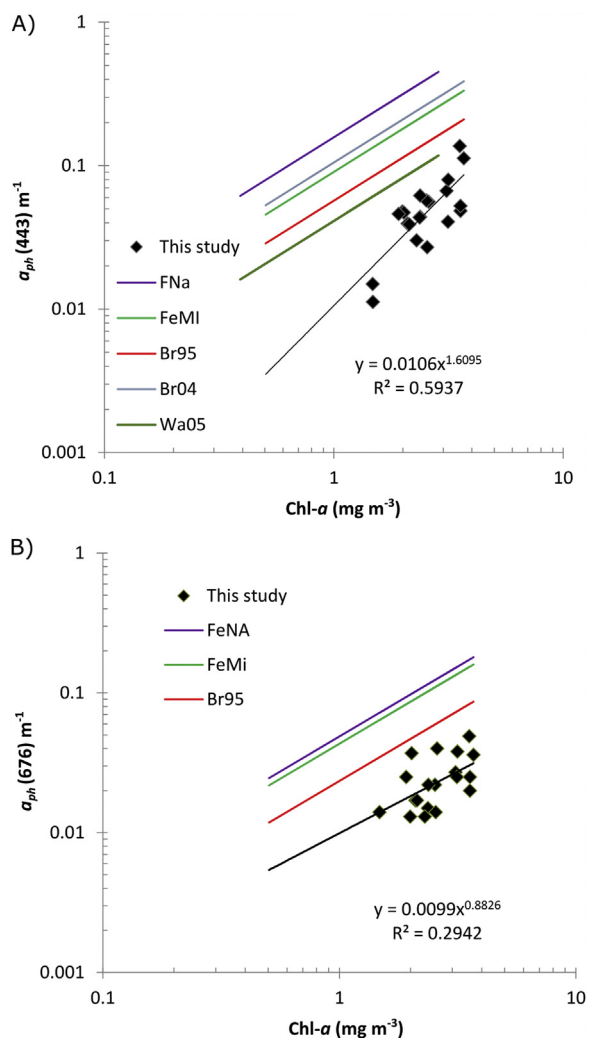
Fig. 5. Variations of the A) a_{ph} (443; m^{-1}) and B) a_{ph} (676; m^{-1}) as a function of Chl-a concentration (mg m^{-3}) for the data collected in this study (black diamonds). Regression lines for the fitting (black) and from previous works are shown: FNa and FeMI (Ferreira et al., 2013b) for Nano-(purple) and Micro-phytoplankton (green), respectively; Wa05 (Wang et al., 2005) in dark green; Br95 in red (Bricaud et al., 1995) and Br04 in light blue (Bricaud et al., 2004). (For interpretation of the references to color in this figure legend, the reader is referred to the web version of this article.)

important to note that the narrow Chl-a range, typical of the studied area, highlights the scattering in the Chl-a concentrations between 1 and 2.5 mg m^{-3}. As in earlier studies, *e.g.* Ciotti et al. (2002) and Bricaud et al. (1995), it was found that diatom-dominated phytoplankton communities had relatively lower values of $a_{ph}*$ in the blue region of the spectrum and thus in these communities an increase in Chl-a concentration was associated with a decrease in $a_{ph}*$ (Fig. 7). According to Ciotti et al. (2002), as phytoplankton cell abundance increases, larger cells would add to a background of smaller cells leading to pigment packaging, *i.e.* decreasing $a_{ph}*$, and an inverse relationship between Chl-a and $a_{ph}*$ is expected.

The shape of the different absorption spectra are influenced by the dominant phytoplankton size classes. Even though all samples were dominated in abundance by the microphytoplankton (40–90%), in some cases the nanophytoplankton presented high abundances (20–50%). In those samples where relatively, high numbers of cocolitophorids appeared, the spectra showed higher absorptions and a more pronounced peak at 443 nm (*e.g.* Fig. 8: MH9, December 2014; MH16, September 2015). On the other hand, in samples where nanoplankton presented lower abundances (20%), the spectra tended to be flatter (*e.g.*

Fig. 8A: MH1, November 2013). It has been previously reported that when cell sizes increase, the spectra flatten consistently with the increase in pigment packaging (Bricaud et al., 1995; Ciotti et al., 2002). Considering the previously referenced studies (*i.e.* Ferreira et al., 2013b; Bricaud et al., 1995; Ciotti et al., 2002), and the spectral curves reported for phytoplankton communities dominated by different cell sizes, the absorption curves obtained in our work resembled those observed under the presence of nanophytoplankton and microphytoplankton. Furthermore, Ciotti et al. (2002) denoted that the variability of the spectral shape in phytoplankton absorption coefficient between 400 and 700 can be explained by the main size dominant phytoplankton. The values for the ratio of the blue-to-red absorption peak in our study (Fig. 8B) also denoted the presence of the two main size-fractions, since it is lower than the ones observed for pure nanoplankton samples and slightly higher than pure microplankton samples (Ferreira et al., 2013b; Ciotti et al., 2002). It is also important to notice that in this same area, Negri et al. (2013) addressed the notorious presence of ultraplankton in the phytoplankton, represented by relatively high abundances of *Synechococcus* and picophytoeukaryotes in February 2011. Thus, the obtained absorption spectra might evidence the influence of these smaller species superimposed to the cell abundances within the size classes considered in this work.

It is well known that bio-optical characteristics of phytoplankton are related to the environmental conditions to which the cells are exposed to, so associations between environmental characteristics (*e.g.* variations in turbidity, water temperature or salinity) and cell sizes and pigment composition are expected. From our results, no clear patterns emerged regarding the environmental controls on phytoplankton composition and dynamics nor optical properties, but these variations are complex and may depend on yet unstudied interactions with environmental and biological components of the ecosystem (Lutz et al., 2006). In addition, it has to be taken into account that a biological property measured at a time might be influenced by acclimation to previous conditions and may not respond to the environmental scenario at the sampling time.

3.5. Evaluation of satellite-derived absorption coefficient

From the 28 oceanographic campaigns, 23 phytoplankton absorption coefficient spectra were measured. Due to cloud cover, the number of match ups was reduced approximately to 12, depending on the atmospheric correction algorithm considered.

3.5.1. NIR, SWIR and combined atmospheric correction algorithms

It is well known that differences between *in situ* and satellite-derived ocean color products may arise due to problems with the atmospheric correction (Williams et al., 2013). Due to lack of *in situ* radiometric measurements, the evaluation of both atmospheric correction algorithms was performed comparing the derived absorption products. At first the three algorithms(GIOP, GSM and QAA) were analyzed applying NIR and SWIR to whole data. No significant differences were observed between both algorithms results (Table 2). Even though the regressions results were slightly better when applying the NIR algorithm ($0.36 < R^2$NIR < 0.48; $0.33 < R^2$SWIR < 0.56), the statistical errors were higher (30% < BIAS-NIR < 68%; 24% < BIAS-SWIR < 60%).

Since the sampled stations varied in total depth (z), distance from the coast, turbidity and suspended sediment matter concentration (Fig. 1), it was decided to evaluate the combined NIR/SWIR algorithm performance by applying each depending of the location of sampling. As the more coastal stations (< 10 km, z ≈ 5 m), red spots in Fig. 1, are characterized by more turbid waters (mean SPM= 58 mg l^{-1}, Turbidity = 10 NFU) SWIR atmospheric correction algorithm was applied while NIR algorithm was applied and in the more distant stations (> 20 km, z > 10 m), cyan spots in Fig. 1, which presented clearer (less turbid) waters (mean SPM = 50 mg l^{-1}, Turbidity = 8 NFU). The standard atmospheric correction algorithm relies on the assumption of
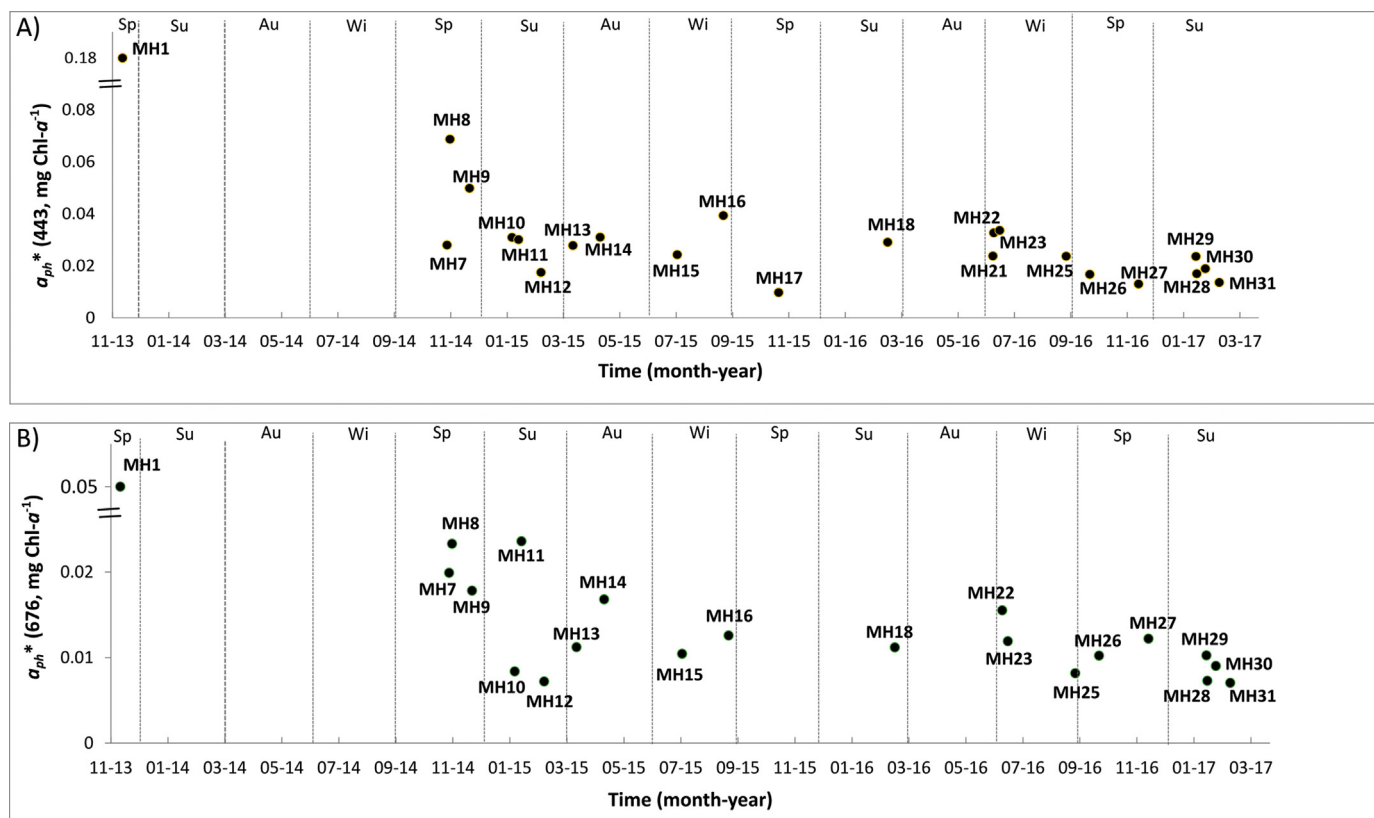
Fig. 6. Daily *insitu* values of A)a_{ph}*(443; mg Chl-a)$^{-1}$ and B)a_{ph}*(676; mg Chl-a)$^{-1}$. Vertical dashed lines delimit seasons: Spring (Sp); Summer (Su); Autumn (Au); Winter (Wi).

negligible water-leaving reflectance in the near-infrared (NIR) region of the spectrum. However, under high suspended sediment conditions their contribution in the NIR might not be negligible (Stumpf et al., 2003; Bailey et al., 2010). In turn, the atmospheric correction algorithm that uses the short-wave infrared (SWIR) bands assumes a negligible water-leaving radiance in this part of the spectrum (Wang, 2007), and has shown a better performance in complex coastal waters (Wang and Shi, 2005; Wang, 2007; Wang et al., 2007, 2009).

Applying the combined NIR/SWIR atmospheric correction algorithm, according to the location of the station (and turbidity and SPM concentration), the regression of all bio-optical algorithms dramatically improved (Table 2). The R^2 ranged between 0.55 and 0.76, meanwhile the error in the estimation (BIAS) varied between 19% and 51%, showing a better performance than applying a single atmospheric correction algorithm to the whole data set (Table 2).

Another possible source of error on the satellite-derived phytoplankton absorption coefficient is the presence of absorption by other specific types of aerosols in the atmosphere which are not currently considered in the models used for atmospheric correction. Previous studies have reported dust emissions in the Patagonian region, which are characterized for following a seasonal pattern, with highest dust activity in summer (Gaiero et al., 2003; Johnson et al., 2011). Moreover, it has been shown that Northern Patagonia became one of the most worldwide active dust sources as a result of poor livestock management and drought conditions (Geist and Lambien, 2004; McConnell et al., 2007). For our match-up data, the aerosol optical thickness (AOT) at 855 nm was analyzed, since it is proportional to aerosol particulate concentration from the ocean surface to the top of the atmosphere. AOT varied between 0.02 and 0.16, evidencing relatively clear atmospheric conditions, *i.e.* AOT < 0.2 (Kwiatkowska, 2003), thus although it would be possible, no evidence of the presence of a dust plume was found during the sampling dates.

3.5.2. Evaluation of a_{ph}(443) products

The a_{ph}(443) products using GIOP, GSM and QAA algorithms using the combined NIR/SWIR atmospheric correction (Section 3.5.1) were analyzed. For the GIOP algorithm a total of 7 match-ups were obtained. The regression analysis presented an R^2 of 0.68, with an intercept of 0.4 and a slope of 0.92. The match-ups are scattered and located relatively far from the 1:1 line, denoted also in the error estimations (Bias = 51%, RMSE = 0.54) (Fig. 9, Table 2). GIOP estimates provided statistically significant regression models with acceptable goodness of fit, the regression line has a slope closer to 1, but a_{ph} (443) values are well above the 1:1 line, indicating a clear overestimation of *in situ* values in all cases (443) (Fig. 9, Table 2).

For the GSM algorithm, regression statistics results are better than for the GIOP algorithm (R^2 = 0.76), but the overestimation is still evident (Bias = 58%) (Fig. 9, Table 2). Both GIOP and GSM algorithms largely overestimated *in situ* values, but errors were higher for GSM regressions and therefore GSM a_{ph} (443) values are further from the 1:1 line for higher *in-situ* values (Fig. 9). GSM and GIOP a_{ph} estimates consider a single value for the specific absorption by phytoplankton coefficient (a_{ph}*) at 443 nm (0.0558 m^2 mg^{-1}), while in our study area the mean value is 0.027 (m^2 mg Chl-a)$^{-1}$, which is the half of what assumed by both algorithms. This value is known to be highly variable since it relies on differences in algal cell size and pigment composition as mentioned before. Lower values of a_{ph}* than the one used for the algorithms parameterization would result in higher estimates of a_{ph} as can be observed in this study (Fig. 8). Furthermore, we addressed the fact that a_{ph}* is not constant in natural waters and that the spectrum assumed in the model might differ from local values (Maritorena et al., 2002).

Regarding QAA performance, the regression line was significant, with an R^2 of 0.55. Comparing to the GIOP and GSM results, QAA estimates were closer to the 1:1 line, but with a slope different from 1, and the estimation errors were lower (Bias = 19%). QAA does not
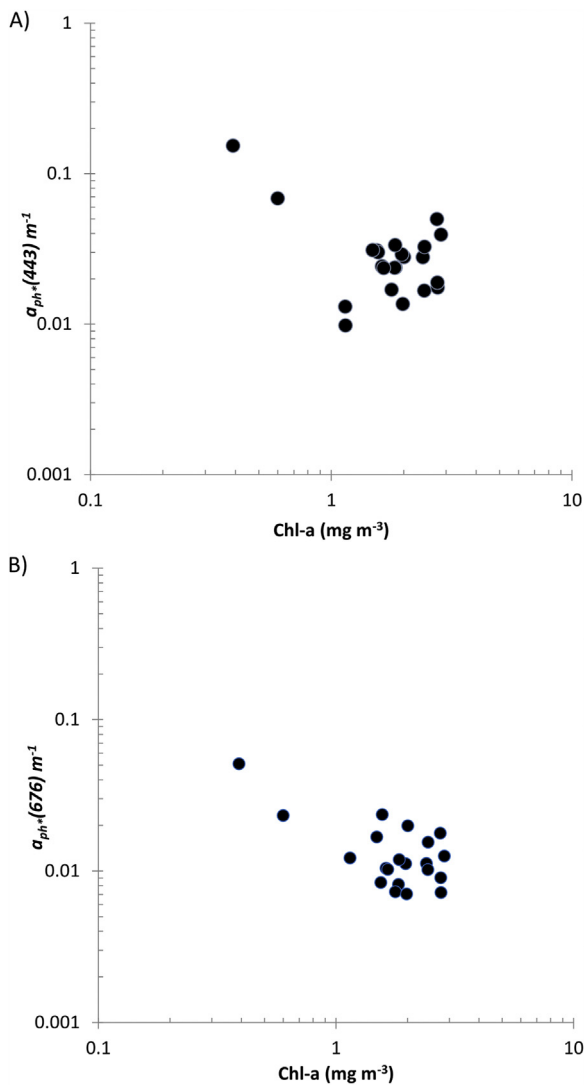
Fig. 7. Variations of the specific absorption coefficient of phytoplankton ($a_{ph}*$): A) at 443 nm and B) 676 nm ($m^2(mgChl-a)^{-1}$) as a function of Chl-a concentration.

Fig. 8. A) Spectral shape of phytoplankton absorption coefficient ($a_{ph}(\lambda)$) and B) mean (full line) and standard deviation (dashed line) spectra of phytoplankton absorption coefficient normalized by the average value of absorption between 400 and 700 nm.

employ spectral models of the $a_{ph}(\lambda)$, only the $a_{ph}(412)/a_{ph}(443)$ ratio is determined through a reflectance band ratio algorithm, but this value could be subsequently modified to keep $a_{ph}(443)$ between 15% and 60% of the total absorption ($a(\lambda)$). So, the a_{ph} spectrum is mostly computed by difference between the total, $a(\lambda)$, and the detrital material or gelbstoff absorption, $a_{dg}(\lambda)$, and thus might be, as a consequence, affected by uncertainties estimating $a(\lambda)$ (Mélin et al., 2007). In our study, even though QAA had a low R^2 and a slope very different from 1, mainly due to one point with a low $a_{ph}(443)$, statistical errors were low and the predictions were closer to *in situ* $a_{ph}(443)$ values.

It can be speculated that marked differences between *in situ* and satellite $a_{ph}(443)$ observed in some dates could be caused by the type of phytoplankton present at that time. As extensively discussed in Section 3.4., variations in the shape of the absorption spectra of phytoplankton were significantly related to the structure of phytoplankton community, mainly to the cell-size. Chain-forming diatoms are the dominant phytoplankton group in this study, characterized by large cells and a relatively low specific absorption that deviates from what is normally assumed in algorithms. In addition, the coccolitophorid *G. oceanica* is a common species that appeared in most samples and reached up to 53% of the phytoplankton cell abundance. This species is characterized for its small size and round shape and the presence of a calcified external

Table 2
Statistical results of the performance of the three bio-optical algorithms GIOP, GSM and QAA, to estimate measured a_{ph} (443), considering two atmospheric correction algorithms, NIR and SWIR and the combination of both (applying SWIR to very coastal stations and NIR to deeper stations). The R^2, derived from linear regression analysis on log-transformed data. RMSE = Root mean square error, RE = Relative error, N = Number of match-ups.

Bio-optical algorithm		NIR	SWIR	SWIR/NIR
GIOP	R^2	0.48	0.4	0.68
	BIAS (%)	52	41	51
	RSME	0.56	0.47	0.54
	RE	2.5	1.16	2.37
	N	8	7	7
GSM	R^2	0.55	0.56	0.76
	BIAS (%)	68	60	58
	RSME	0.73	0.68	0.71
	RE	3.9	3.93	2.91
	N	9	9	9
QAA	R^2	0.36	0.33	0.55
	BIAS (%)	30	24	19
	RSME	0.36	0.32	0.29
	RE	1.11	0.82	0.3
	N	12	13	12

cell structure which is known to be responsible of causing high back scattering on satellite images (Brown and Yoder, 1994). From the analyses it was observed that match-ups located farther from the 1:1 line coincide with relatively higher abundance of *G. oceanica* in the sample or relatively high $a_{ph}(443)$ coefficient. Additional uncertainties in the match-up may be associated with imperfections in the
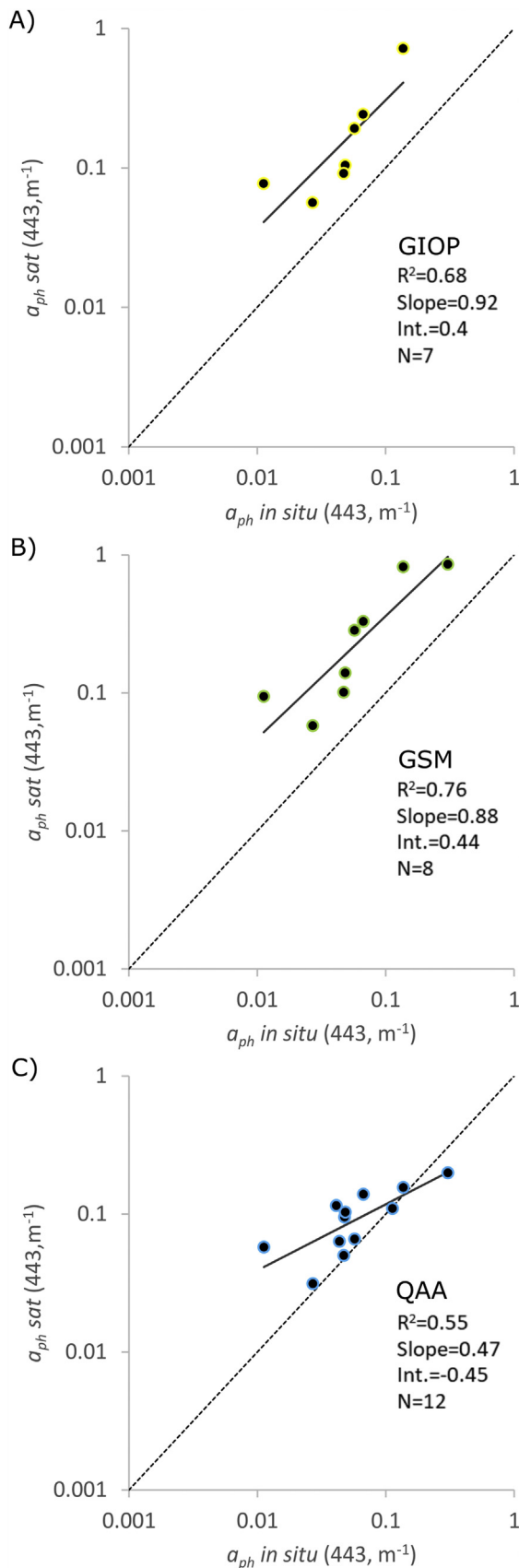
Fig. 9. Comparison between *in situ* measured and satellite-derived absorption by phytoplankton at 443 nm using the A) GIOP, B) GSM and C) QAA algorithms with NIR and SWIR atmospheric correction algorithms. The coefficient of determination (R^2), slope, intercept (Int.) and number of match-ups (N) are shown.

atmospheric correction of satellite images over coastal waters (Shang et al., 2011), as mentioned before but could not be analyzed with the available *in situ* data.

4. Conclusions

El Rincón is characterized by highly turbid waters all year round and for presenting a wide seasonal range of temperature and salinity. This area is influenced by the estuarine plume coming from the neighbor Bahía Blanca Estuary, and is subjected to constant winds which promote mixed water conditions all year round. Phytoplankton groups responded to this variable environment, dominated by chain-forming diatoms in the microplankton size class which are typical of turbulent turbid coastal waters. Second in abundance was the nano-plankton size class, composed by a single species of cocolitophorids, whose morphological and physiological particularities provide ecological advantages under highly fluctuating environments. During the three-year study, no clear seasonality in the phytoplankton abundance was found. This suggests that local environmental forces, like under-water light availability, might be driving the phytoplankton development in these mixed coastal waters. The absorption of phytoplankton coefficient values for a given Chl-*a* concentration were considerably lower than in other regions of the world, which could be explained by the dominance of large species and their photoacclimation to low light conditions in these coastal waters. Hence, the compound effects of shallow and highly turbid waters, high temporal variability in the phytoplankton composition and evidence of cells' packaging effect, highlight the limitation of traditional bio-optical models to parameterize the phytoplankton components in terms of total Chl-*a* concentration.

Despite the complexity of El Rincón waters, reasonable results were found when comparing the bio-optical estimates with *in situ* data. Because the sampling sites varied in location, depth and turbidity/SPM applying either SWIR or NIR, depending on the location of the samples, more accurate results were found. Overall, GIOP and GSM algorithms reflected the general tendency (slope close to one), but they both considerably overestimated *in situ* a_{ph}(443) values. Acknowledging that there is an over estimation, seasonal and inter-annual variability could be reproduced. In turn, QAA algorithm showed a better performance in retrieving a_{ph}(443)with lower estimation errors although regression analysis showed lower accuracy than the other algorithms.

The results found reinforce the typical uncertainty of applying global algorithms to regional or local scales. Our results, which clearly differ from other regions of the world, suggest that a regional calibration of the mentioned algorithms might be necessary, but this needs more *in situ* measurements. This study is a first step in the optical characterization of El Rincón coastal waters and reinforces the need of a detailed characterization of these complex waters to develop and improve regional algorithms for ocean color remote sensing.

References

Ahn, Y.H., Shanmugam, P., Moon, J.E., 2006. Retrieval of ocean colour from high

resolution multi-spectral imagery for monitoring highly dynamic ocean futures. Int. J. Remote Sens. 27, 367–392.

Bailey, S.W., Werdell, P.J., 2006. A multi-sensor approach for the on-orbit validation of ocean color satellite data products. Remote Sens. Environ. 102, 12–23. https://doi.org/10.1016/ j.rse.2006.01.015.

Bailey, S.W., Franz, B.A., Werdell, P.J., 2010. Estimation of near-infrared water-leaving reflectance for satellite ocean color data processing. Opt. Express 18 (7), 7521–7527.

Bouman, J., de Koter, A., Dominik, C., Waters, L.B.F.M., 2003. The origin of crystalline silicates in the Herbig Be star HD 100546 and in comet Hale-Bopp. Astron. Astrophys. 401 (2), 577–592.

Brewin, R.J., Hirata, T., Hardman-Mountford, N.J., Lavender, S.J., Sathyendranath, S., Barlow, R., 2012. The influence of the Indian Ocean Dipole on interannual variations in phytoplankton size structure as revealed by Earth Observation. Deep Sea Res. Part II: Top. Stud. Oceanogr. 77, 117–127.

Bricaud, A., Babin, M., Morel, A., Claustre, H., 1995. Variability in the chlorophyll-specific absorption coefficients of natural phytoplankton: analysis and parameterization. J. Geophys. Res. 100, 13321–13332.

Bricaud, A., Claustre, H., Ras, J., Oubelkheir, K., 2004. Natural variability of phytoplanktonic absorption in oceanic waters: influence of the size structure of algal populations. J. Geophys. Res.: Oceans 109 (C11).

Brown, C.W., Yoder, J.A., 1994. Distribution pattern of coccolithophorid blooms in the western North Atlantic Ocean. Cont. Shelf Res. 14 (2), 175–197.

Brzezinski, M.A., Villareal, T.A., Lipschultz, F., 1998. Silica production and the contribution of diatoms to new and primary production in the central North Pacific. Mar. Ecol. Prog. Ser. 167, 89–104.

Campbell, J.W., 1995. The lognormal distribution as a model for bio-optical variability in the sea. J. Geophys. Res. 100, 13237–13254.

Carroza, C., Aráoz, N.F., Pájaro, M., 2009. Variado costero y su interacción con especies pelágicas. Inf. Asesor. Transf. INIDEP 2/09, 6.

Ciotti, A.M., Cullen, J.J., Lewis, M.R., 1999. A semi-analytical model of the influence of phytoplankton community structure on the relationship between light attenuation and ocean color. J. Geophys. Res. 104, 1559–1578.

Ciotti, A.M., Lewis, M.R., Cullen, J.J., 2002. Assessment of the relationships between dominant cell size in natural phytoplankton communities and the spectral shape of the absorption coefficient. Limnol. Oceanogr. 47 (2), 404–417.

Clemenston, L.A., Parslow, J.S., Turnbull, A.R., Bonham, P.I., 2004. Properties of light absorption in a highly coloured estuarine system in south-east Australia which is prone to blooms of the toxic dinoflagellate *Gymnodinium catenatum*. Estuar. Coast. Shelf Sci. 60, 101–112.

Delgado, A.L., Vitale, A.J., Perillo, G.M., Piccolo, M.C., 2012. Preliminary analysis of waves in the coastal zone of Monte Hermoso and Pehuén Co, Argentina. J. Coast. Res. 28 (4), 843–852.

Delgado, A.L., Jamet, C., Loisel, H., Vantrepotte, V., Perillo, G.M.E., Piccolo, M.C., 2014. Evaluation of the MODIS-Aqua Sea-Surface Temperature product in the inner and mid-shelves of southwest Buenos Aires Province, Argentina. Int. J. Remote Sens. 35 (1), 306–320. https://doi.org/10.1080/01431161.2013.870680.

Delgado, A.L., Menéndez, M.C., Piccolo, M.C., Perillo, G.M.E., 2017. Hydrography of the inner continental shelf along the Southwest Buenos Aires Province, Argentina: influence of an Estuarine Plume on Coastal Waters. J. Coast. Res. 907–916. https://doi.org/10.2112/JCOASTRES-D-16-00064.1.

Dupouy, C., Neveux, J., Ouillon, S., Frouin, R., Murakami, H., Hochard, S., Dirberg, G., 2010. Inherent optical properties and satellite retrieval of chlorophyll concentration in the lagoon and open ocean waters of New Caledonia. Mar. Pollut. Bull. 61, 503–518.

Ferreira, A., Garcia, C.A.E., Dogliotti, A.I., Garcia, V.M.T., 2013a. Bio-optical characteristics of the Patagonia Shelf break waters: implications for ocean color algorithms. Remote Sens. Environ. 136, 416–432.

Ferreira, A., Stramski, D., Garcia, C.A.E., Garcia, V.M.T., Ciotti, A.M., Mendes, C.R.B., 2013b. Variability in light absorption and scattering of phytoplankton in Patagonian waters: role of community size structure and pigment composition. J. Geophys. Res.: Oceans 118, 698–714.

Field, C.B., Behrenfeld, M.J., Randerson, J.T., Falkowski, P., 1998. Primary production of the biosphere: integrating terrestrial and oceanic components. Science 281 (5374), 237–240.

Finkel, Z.V., Beardall, J., Flynn, K.J., Quigg, A., Rees, T.A.V., Raven, J.A., 2009. Phytoplankton in a changing world: cell size and elemental stoichiometry. J. Plankton Res. 32 (1), 119–137.

Franz, B.A., Werdell, P.J., 2010. A generalized framework for modeling of inherent optical properties in ocean remote sensing applications, Proceedings of Ocean Optics XX, Anchorage, Alaska, 27th Sept.–1st Oct.

Gaiero, D.M., Probst, J.L., Depetris, P.J., Bidart, S.M., Leleyter, L., 2003. Iron and other transition metals in Patagonian riverborne and windborne materials: geochemical control and transport to the southern South Atlantic Ocean. Geochim. Cosmochim. Acta 67 (19), 3603–3623.

Geist, H.J., Lambien, E.F., 2004. Dynamic causal patterns of desertification. Bioscience 54, 817–829.

Gordon, H.R., Brown, O.B., Evans, R.H., Brown, J.W., Smith, R.C., Baker, K.S., Clark, D.K., 1988. A semianalytic radiance model of ocean color. J. Geophys. Res. 93, 10909–10924.

Guinder, V.A., Popovich, C.A., Perillo, G.M., 2009. Particulate suspended matter concentrations in the Bahía Blanca estuary, Argentina: implication for the development of phytoplankton blooms. Estuar. Coast. Shelf Sci. 85 (1), 157–165.

Guinder, V.A., Tillmann, U., Krock, B., Delgado, A.L., Krohn, T., Garzón Cardona, J.E., Metfies, K., López Abbate, C., Silva, R., Lara, R., 2018. Plankton multiproxy analyses in the Northern Patagonian shelf, Argentina: community structure, phycotoxins and characterization of Alexandrium strains. Front. Mar. Sci. https://doi.org/10.3389/fmars.2018.00394.

Hasle, G., 1978. Concentrating phytoplankton. Settling: the inverted microscope method. In: Sournia, A. (Ed.), Phytoplankton Manual. Monographs on Oceanographic Methodology, vol. 6. UNESCO, Paris, pp. 88–96.

Hillebrand, H., Dürselen, C.D., Kirschtel, D., Pollingher, U., Zohary, T., 1999. Biovolume calculation for pelagic and benthic microalgae. J. Phycol. 35, 403–424.

Hirawake, T., Takao, S., Horimoto, N., Ishimaru, T., Yamaguchi, Y., Fukuchi, M., 2011. A phytoplankton absorption-based primary productivity model for remote sensing in the Southern Ocean. Polar Biol. 34, 291–302.

Hoepffner, N., Sathyendranath, S., 1992. Bio-optical characteristics of coastal waters: absorption spectra of phytoplankton and pigment distribution in the western North Atlantic. Limnol. Oceanogr. 37, 1660–1679.

Holm-Hansen, O., Lorenzen, C.J., Holmes, R.W., Strickland, J.D.H., 1965. Fluorometric determination of chlorophyll. J. Cons. Perm. Int. Explor Mer. 30, 3–15.

Hoppenrath, M., Debres, G., 2009. Marine phytoplankton. Selected microplankton species from the North Sea around Helgoland and Sylt. E. Schweizerbart'scheVerlagsbuchhandlung, 264 pp.

Jamet, C., Loisel, H., Kuchinke, C.P., Ruddick, K., Zibordi, G., Feng, H., 2011. Comparison of three SeaWiFS atmospheric correction algorithms for turbid waters using AERONET-OC measurements. Remote Sens. Environ. 115, 1955–1965. https://doi.org/10.1016/j.rse.2011.03.018.

Johnson, M.S., Meskhidze, N., Kiliyanpilakkil, V.P., Gasso, S., 2011. Understanding the transport of Patagonian dust and its influence on marine biological activity in the South Atlantic Ocean. Atmos. Chem. Phys. 11, 2487–2502.

Johnsen, G., Samset, O., Granskog, L., Sakshaug, E., 1994. In vivo absorption characteristics in 10 clases of bloom-forming phytoplankton: taxonomic characteristics and responses of photoadaptation by means of discriminant and HPLC analysis. Mar. Ecol. Prog. Ser. 105, 149–157.

Kai, M., Hara, T., Aoyama, H., Kurod, A.N., 1999. A massive coccolithophorid bloom observed in Mika wa Bay, Japan. J. Oceanogr. 55 (3), 395–406.

Kishino, M., Takahashi, M., Okami, N., Ichimura, S., 1985. Estimation of the spectral absorption coefficients of phytoplankton in the sea. Bull. Mar. Sci. 37, 634–642.

Kwiatkowska, E., 2003. Comparisons of daily global ocean color datasets: MODIS Terra/Aqua and SeaWiFS. In: Fargion, G.S., McClain, C.R. (Eds.), MODIS Validation, Data Merger and Other Activities Accomplished by SIMBIOS Project: 2002–2003, TM-2003, SIMBIOS Project. NASA Goddard Space Flight Center, Greenbelt, M.D., pp. 2–18.

Lee, Z., Carder, K.L., Arnone, R.A., 2002. Deriving inherent optical properties from water color: a multiband quasi-analytical algorithm for optically deep waters. Appl. Opt. 41 (27), 5755–5772.

Lee, Z., Lance, V.P., Shang, S., Vaillancourt, R., Freeman, S., Lubac, B., Hargreaves, B.R., Del Castillo, C., Miller, R., Twardowski, M., Wei, G., 2011. An assessment of optical properties and primary production derived from remote sensing in the Southern Ocean (SO GasEx). J. Geophys. Res.: Oceans 116 (C4).

Legendre, L., 1990. The significance of microalgal blooms for fisheries and for the export of particulate organic carbon in oceans. J. Plankton Res. 12 (4), 681–699.

Litchman, E., Edwards, K.F., Klausmeier, C.A., Thomas, M.K., 2012. Phytoplankton niches, traits and eco-evolutionary responses to global environmental change. Mar. Ecol. Prog. Ser. 470, 235–248.

Longhurst, A., Sathyendranath, S., Platt, T., Caverhill, C., 1995. An estimate of global primary production in the ocean from satellite radiometer data. J. Plankton Res. 17 (6), 1245–1271.

López Cazorla, A., Molina, J.M., Ruarte, C., 2014. The artisanal fishery of *Cynoscion guatucupa* in Argentina: exploring the possible causes of the collapse in Bahía Blanca estuary. J. Sea Res. 88, 29–35.

Lucas, A.J., Guerrero, R.A., Mianzán, H.W., Acha, E.M., Lasta, C.A., 2005. Coastal oceanographic regimes of the northern Argentine continental shelf (34–43 S). Estuar. Coast. Shelf Sci. 65, 405–420.

Lutz, V.A., Subramaniam, A., Negri, R.M., Silva, R.I., Carreto, J.I., 2006. Annualvariations in bio-opticalpropertiesatthe Estacion Permanente de EstudiosAmbientales (EPEA) coastal station, Argentina. Cont. Shelf Res. 26, 1093–1112.

Margalef, R., 1978. Life forms of phytoplankton as survival alternatives in an unestable environment. Oceanol. Acta 1, 493–509.

Marra, J., Trees, C.C., O'Reilly, J.E., 2007. Phytoplankton pigment absorption: a strong predictor of primary productivity in the surface ocean. Deep Sea Res. I 54, 155–163.

McConnell, J.R., Aristarain, A.J., Banta, J.R., Edwards, P.R., Simoes, J.C., 2007. 20th-Century doubling in dust achieve in an Antartic Peninsula ice core parallels climate change and desertification in South America. Proc. Natl. Acad. Sci. USA 104, 5743–5748.

Maritorena, S., Siegel, D.A., PetersonA, R., 2002. Optimization of a semianalytical ocean color model for global scale application. Appl. Opt. 41, 2705–2714.

Mélin, F., Zibordi, G., Berthon, J.F., 2007. Assessment of satellite ocean color products at a coastal site. Remote Sens. Environ. 110, 192–215.

Menden-Deuer, S., Lessard, E.J., 2000. Carbon to volume relationships for dinoflagellates, diatoms, and other protist plankton. Limnol. Oceanogr. 45 (3), 569–579.

Mitchell, B.G., 1990. Algorithms for determining the absorption coefficient for aquatic particulates using the quantitative filter technique. In: *Ocean optics X*. International Society for Optics and Photonics, 1302, pp. 137–149.

Mitchell, B.G., Bricaud, A., Carder, K., 2000. Determination of spectral absorption coefficients of particles, dissolved material and phytoplankton for discrete water samples. In: Fargion, G.S., Muller, J.L. (Eds.), Ocean Optics Protocols for Satellite Ocean Color Sensor Validation, revision 2. NASA Goddard Space Flight Space Center, Greenbelt, Maryland, pp. 125–153.

Moisan, T.A., Mitchell, B.G., 1999. Photophysiological acclimation of *Phaeocystis antarctica* Karsten under light limitation. Limnol. Oceanogr. 44, 247–258.

Morel, A., Bricaud, A., 1981. Theoretical results concerning light absorption in a discrete

medium, and application to specific absorption of phytoplankton. Deep Sea Res. 28, 1375–1393. https://doi.org/10.1016/0198-0149(81)90039-X.

Negri, R.M., Silva, R.I., Segura, V.A., Cucchi Colleoni, A.D., 2013. Estructura de la comunidad del fitoplancton en el área de El Rincón, Mar Argentino (febrero 2011). Rev. de Invest. y Desarro. Pesq. 23, 7–22.

Perillo, G.M.E., Cuadrado, D.G., 1990. Near surface suspended sediments in Monte Hermoso Beach, Argentina: I. descriptive characteristics. J. Coast. Res. 6 (4), 981–990.

Piccolo, M.C., 1998. Oceanography of the western South Atlantic continental shelf from 33 to 55°S. The sea, 11, pp. 253–271.

Redfield, A.C., Ketchum, B.H., Richards, F.A., 1963. The influence of organisms on the composition of sea-water. En: Hill, M.N. (Ed.), The Sea, Interscience, 2, pp. 26–77.

Rohdes, L.L., Peake, B.M., Mackenzie, A.L., Marwick, S., 1995. Coccolithophores *Gephyrocapsa oceanica* and *Emiliania huxleyi* (Prymnesiophyceae = Haptophyceae) in new Zealand's coastal waters: characteristics of blooms and growth in laboratory culture. New Zeland J. Mar. Freshw. Res. 29 (3), 345–357.

Sathyendranath, S., Cota, G., Stuart, V., Maas, H., Platt, T., 2001. Remote Sensing of phytoplankton pigments: a comparison of empirical and theoretical approaches. Int. J. Remote Sens. 22, 249–273. https://doi.org/10.1080/014311601449925.

Sathyendranath, S., Watts, L., Devred, E., Platt, T., Caverhill, C., Maass, H., 2004. Discrimination of diatoms from other phytoplankton using ocean-colour data. Mar. Ecol. Prog. Ser. 272, 59–68.

Segura, V., Lutz, V.A., Dogliotti, A., Silva, R.I., Negri, R.M., Akselman, R., Benavides, H., 2013. Phytoplankton types and primary production in the Argentine Sea. Mar. Ecol. Prog. Ser. 491, 15–31.

Shang, S., Dong, Q., Lee, Z., Li, Y., Xie, Y., Behrenfeld, M., 2011. MODIS observed phytoplankton dynamics in the Taiwan Strait: an absorption-based analysis. Biogeosciences 8, 841–850.

Shang, S.L., Dong, Q., Hu, C.M., Lin, G., Li, Y.H., Shang, S.P., 2014. On the consistency of MODIS chlorophyll a products in the northern South China Sea. Biogeosciences 11, 269–280.

Sommer, U. (Ed.), 2012. Plankton Ecology: Succession in Plankton Communities. Springer Science & Business Media.

Stramski, D., Boss, E., Bogucki, D., Voss, K., 2004. The role of seawater conctituents in light backscattering in the ocean. Prog. Oceanogr. 61, 27–56.

Stramski, D., Bricaud, A., Morel, A., 2001. Modeling the inherent optical properties of the ocean based on the detailed composition of the planktonic community. Appl. Opt. 40,

2929–2945. https://doi.org/10.1364/AO.40.002929.

Stumpf, R.P., Arone, R.A., Gould, R.W., Ransibrahmanakul, V., 2003. A partially coupled ocean-atmosphere model for retrieval of water-leaving radiance from SeaWiFS in coastal waters. In: Hooker, S.B., Firestone, E.R. (Eds.), SeaWiFS Postlaunch Technical Report Series Chap.9, NASA/TM-2003-206892, vol. 22. NASA Goddard Space Flight Space Center, Greenbelt, Maryland, pp. 51–59.

Van der Linde, D.W., 1998. Protocol for determination of total suspended matter in oceans and coastal zones. Joint Research Centre, Ispra. Technical note 1.98.182.

Van de Waal, D.B., Verschoor, A.M., Verspagen, J.M., van Donk, E., Huisman, J., 2010. Climate-driven changes in the ecological stoichiometry of aquatic ecosystems. Front. Ecol. Environ. 8 (3), 145–152.

Vantrepotte, V., Brunet, C., Mériaux, X., Lécuyer, E., Velluci, V., Santer, R., 2007. Biooptical properties of coastal Waters in the Eastern English Channel. Estuar. Coast. Shelf Sci. 72, 201–212.

Wang, M., 2007. Remote sensing of the ocean contributions from ultraviolet to nearinfrared using the shortwave infrared bands: simulations. Appl. Opt. 46, 1535–1547.

Wang, J., Cota, G.F., Ruble, D.A., 2005. Absorption and backscattering in the Beaufort and Chukchi Seas. J. Geophys. Res. 110, C04014.

Wang, M., Shi, W., 2005. Estimation of ocean contribution at the MODIS near-infrared wavelengths along the East coast of the U.S.: two case studies. Geophys. Res. Lett. 32, L13606.

Wang, M., Shi, W., 2007. The NIR-SWIR combined atmospheric correction approach for MODIS ocean color data processing. Opt. Express 15 (24), 15722–15733.

Wang, M., Tang, J., Shi, W., 2007. MODIS-derived ocean color products along the China east coastal region. Geophys. Res. Lett. 34 (L06611), 1–5. https://doi.org/10.1029/2006GL028599.

Wang, M., Son, S., Harding, L.W.J., 2009. Retrieval of diffuse attenuation coefficient in the Cheseapeake Bay and turbid ocean regions for satellite ocean color applications. J. Geophys. Res. 114 (C10011), 1–15.

Werdell, P.J., Franz, B.A., Bailey, S.W., Feldman, G.C., Boss, E., Brando, V.E., Dowell, M., Hirata, T., Lavender, S.J., Lee, Z., 2013. Generalized ocean color inversion model for retrieving marine inherent optical properties. Appl. Opt. 52, 2019–2037.

Williams, G.N., Dogliotti, A.I., Zaidman, P., Solis, M., Narvarte, M.A., Gonzalez, R.C., Esteves, J.L., Gagliardini, D.A., 2013. Assesment of remotely-sensed sea-surface temperature and chlorophyll-*a* concentration in San Matias Gulf (Patagonia, Argentina). Cont. Shelf Res. 52, 159–171.